Selective sampling using confocal Raman spectroscopy provides enhanced specificity for urinary bladder cancer diagnosis

Massachusetts Institute of Technology

ORIGINAL PAPER

Selective sampling using confocal Raman spectroscopy provides enhanced specificity for urinary bladder cancer diagnosis

**Ishan Barman · Narahara Chari Dingari ·
Gajendra Pratap Singh · Rajesh Kumar ·
Stephen Lang · Ghulam Nabi**

Abstract In recent years, Raman spectroscopy has shown substantive promise in diagnosing bladder cancer, especially due to its exquisite molecular specificity. The ability to reduce false detection rates in comparison to existing diagnostic tools such as photodynamic diagnosis makes Raman spectroscopy particularly attractive as a complementary diagnostic tool for real-time guidance of transurethral resection of bladder tumor (TURBT). Nevertheless, the state-of-the-art high-volume Raman spectroscopic probes have not reached the expected levels of specificity thereby impeding their clinical translation. To address this issue, we propose the use of a confocal Raman probe for bladder cancer diagnosis that can boost the specificity of the diagnostic algorithm based on its suppression of the out-of-focus non-analyte-specific signals emanating from the neighboring normal tissue. In this article, we engineer and apply such a probe, having depth of field of approximately 280 μm, for Raman spectral acquisition from ex vivo normal and cancerous TURBT samples. Using this clinical dataset, a diagnostic algorithm based on principal component analysis and logistic regression is developed. We demonstrate that this approach results in comparable sensitivity but significantly higher specificity in relation to high-volume Raman spectral data. The application of only two principal components is sufficient for the discrimination of the samples underlining the robustness of the algorithm. Further, no discordance between replicate spectra is observed emphasizing the reproducible nature of the current diagnostic assessment. The high levels of sensitivity and specificity achieved in this proof-of-concept study opens substantive avenues for application of a confocal Raman probe during endoscopic procedures related to diagnosis and treatment of bladder cancer.

Ishan Barman, Narahara Chari Dingari, and Gajendra Pratap Singh contributed equally to this work.

I. Barman · N. C. Dingari
G. R. Harrison Spectroscopy Laboratory,
Massachusetts Institute of Technology,
Cambridge, MA 02139, USA

G. P. Singh · S. Lang · G. Nabi
Medical Research Institute, University of Dundee,
Dundee, Scotland DD19SY, UK

R. Kumar
Department of Physics, Norwegian University of Science and Technology,
7491 Trondheim, Norway

S. Lang
Department of Pathology, Ninewells Hospital,
Dundee, Scotland DD19SY, UK

G. Nabi (✉)
Academic Section of Urology, Ninewells Hospital,
Dundee, Scotland DD19SY, UK
e-mail: g.nabi@dundee.ac.uk

Introduction

Urinary bladder cancer accounts for 5–10 % of all cancers in the United States and Europe and is the fourth most common cancer in men [1]. The majority of diagnosed patients (75–85 %) suffer from non-muscle invasive disease, which is characterized by a probability of recurrence in the range of 31–78 % within 5 years of initial diagnosis [2]. Currently, flexible cystoscopy and voided urine cytology are employed

for diagnosis of patients with symptoms suggestive of bladder cancer. In particular, if flexible cystoscopy confirms a bladder tumor or urine cytology shows malignant cells in the absence of an upper urinary tract urothelial tumor, a rigid white light cystoscopy (WLC) under general or regional anesthesia is performed with transurethral resection of bladder tumor (TURBT), where applicable.

The ultimate goal in the management of non-muscle invasive transitional cell carcinoma (TCC) of the bladder is the prevention of disease recurrence and progression. Early cancer detection is an essential prerequisite of successful therapy. Unfortunately, small papillary bladder tumors and flat urothelial tumors such as carcinoma in situ (CIS) can easily be overlooked during conventional WLC. Moreover, progression to muscle invasive or metastatic TCC is more likely to occur in those with concomitant CIS [3]. Additionally, while the application of photodynamic diagnosis (PDD) is known to enhance the sensitivity of bladder cancer detection from ca. 75 % (for conventional WLC) to ca. 95 % (for PDD) and increase the recurrence free survival by 67 % [4, 5], significantly larger false detection rates (of the order of 40 %) have impeded the path towards full adoption of this methodology [6–8]. Also, from an economic standpoint, non-muscle invasive TCC of the bladder is one of the most expensive cancers to manage on a per patient basis [9], because of its high prevalence, high recurrence rate and the need for long-term cystoscopic surveillance.

In order to meet the substantive unmet clinical need for an accurate and robust real-time diagnostic tool, several methods including optical imaging and spectroscopy have been explored by investigators over the past decade [10, 11]. In particular, Raman spectroscopy has emerged as one of the promising approaches as it interrogates the molecular composition of the tissue in real time without necessitating the addition of exogenous dyes or labels thereby providing an objective picture of the pathology with minimal perturbation to the sample under investigation. By measuring changes in the wavelength of light scattered from a sample, the biochemical makeup of the tissue may be inferred. In conjunction with multivariate chemometric methodologies that analyze the spectral information available over all the spectral channels [12], Raman spectroscopy has been shown to provide clinically relevant diagnostic information in a wide variety of disease types ranging from atherosclerosis to breast and skin cancer [13–17]. Minimally invasive endoscopic techniques aimed at detection of cancer cells in the lining of the urinary bladder using biophotonic technology such as Raman spectroscopy can interrogate the molecular composition of the cells and provide an objective and highly specific picture of the pathology. In this regard, female patients and patients with a TURBT or/and intravesical adjuvant treatment within 3 months of cystoscopic

examination [18] are likely to receive maximum benefits due to the exquisite specificity of Raman-based diagnosis. This group of patients is at an increased risk of having benign conditions (including inflammation of bladder mucosa), which appears similar to cancer under the white light cystoscopic examination. It is expected that a highly specific technology would provide point measurements using an optical probe and accurately analyze tissues without removing it and, therefore, direct biopsies to areas more likely to contain cancers. In effect, this approach should reduce the number of unnecessary endoscopic biopsies and prevent biopsy related morbidity and cost. We envisage Raman spectroscopy as a complementary diagnostic tool that will work in combination with the existing fluorescence cystoscopy techniques to enhance the overall diagnostic value for bladder cancer determination.

To this end, Stone and co-workers have shown that Raman microscopy can provide sensitivities and specificities >90 % in an eight-group algorithm for bladder tissue samples [19]. The next step in the progression was also taken by the same group when they reported a fiber-optic-based clinical Raman system that was able to discriminate between (snap-frozen) benign and malignant bladder samples with an overall accuracy of 84 % [20]. These foundational works paved the way for in vivo translation of the Raman-based diagnostic approach. In this regard, one of the most promising recent investigations was conducted by Draga and co-workers [21], where they described bladder cancer diagnosis in vivo using high-volume Raman spectroscopic probes. Using multivariate classification models, they have reported the ability to distinguish cancer from normal tissue with a sensitivity of 85 % and specificity of 79 %.

However, the underlying rationale for using Raman spectroscopy resides in the potentially higher specificity of Raman-based diagnosis in relation to PDD or fluorescence cystoscopy. The relatively low specificity of this latest in vivo study presents a substantive challenge to the clinical translation of Raman spectroscopy. The goal of this paper is to make optimal use of the specificity of Raman spectroscopy to substantially reduce the number of false detection rates, even at the risk of slightly comprising on the sensitivity metric. In this context, the large sampling volume of conventional Raman spectroscopy probes has a deleterious diagnostic impact due to the confounding (out-of-focus) signals of the spectral interferents and fluorescence arising from neighboring normal tissue, as also noted by Draga and co-workers [21]. In order to overcome this high (and nonspecific) sampling volume-based constraint, we propose and employ a confocal Raman spectroscopy probe that has a sampling depth of less than 300 μm. We hypothesize that the limited sampling depth of our probe provides a superior platform for measuring the grade and aggressive potential of

tumors typically observed in bladder cancer cases such as carcinoma in situ. In this article, we assess the diagnostic potential of such a system, for the first time, in tumors removed from patients undergoing TURBT. Importantly, we show that this system results in comparable sensitivity to that using high-volume Raman probes but in significantly higher specificity. It is remarkable that such a high value of specificity can be obtained using only two principal components in the diagnostic algorithm, which further emphasizes the robustness of the proposed methodology to noise and potential spurious correlations. The proof-of-concept investigation outlined in this paper should serve as the foundation for future work to establish endoscopic application of confocal Raman spectroscopy in a larger number of patients. We anticipate that in larger clinical datasets, one can not only detect bladder cancer but also demarcate the stage of its invasion using the proposed approach.

Materials and methods

Raman instrumentation

The Raman spectroscopy system used for the ex vivo tissue measurements in this study consists of a 785 nm diode laser (Laser2000, UK) temperature stabilized for Raman excitation, a modified high throughput HoloSpec spectrometer (Kaiser Inc.) and a front illuminated iDUS CCD camera (Andor Inc., UK). The light was delivered to a spot of ca. 1 mm^2 area (where the power at the sample was approximately 60 mW) and collected from the tissue using a Raman probe, whose design is identical to the Motz probe described in detail elsewhere [22, 23]. Briefly, the collection component of our probe consisted of ten tightly packed low-OH 200 μm core optical fibers (Thorlabs Inc.), for Raman signal collection where the low-OH content of the fiber reduces the generation of the large fluorescence signal. In addition, an identical optical fiber of 200 μm core was used for Raman signal excitation. A bandpass filter (Semrock Inc., USA) was used at the tip of the excitation fiber and a longpass filter (Semrock Inc., USA) was used at the tip of collection fibers. The bandpass filter blocks the background generated in the excitation fiber and the longpass filter blocks the laser (and Rayleigh scattered) light entering the collection fibers. A ball lens (Knight Opticals, UK) was used at the tip of the excitation fiber to deliver the light to the tissue. Medical glue (Henkel, Germany) was used for assembly of the various optical and mechanical components in the probe. A steel tube (Small Parts Inc., USA) was utilized for the outermost sheath to add mechanical rigidity to the entire assembly. In the ensuing discussion, we will refer to this probe as the high-volume Raman probe to distinguish it from the confocal variant described below.

As mentioned in the "Introduction", for a probe to be sufficiently specific to analyze the region of interest where cancerous and pre-cancerous cells can be observed, and to preclude the dilution of the Raman signal of this region, it is imperative to develop a probe with limited sampling depth. This issue is addressed by incorporating confocality into the aforementioned high-volume probe. In particular, light from the proximal end of the collection fibers is focused on to a pinhole aperture of diameter 150 μm (Thorlabs Inc.). The light transmitted through the pinhole is collimated and subsequently focused onto the spectrograph slit. Here, the pinhole constitutes the primary confocal aperture (rather than the optical fibers themselves), which enables the increase or decrease of the depth of field by switching to a pinhole of different dimension. Such alteration of depth of field does not require any change in design and fabrication of the Raman fiber probe itself. Additionally, the current design facilitates the acquisition of Raman spectra using both modalities, namely the high-volume and confocal probe, by simply removing/adding the pinhole to the system. This, in turn, permits the direct comparison of the performance of the confocal probe vis-à-vis that of the high-volume one.

The depth of field of both the high-volume and confocal Raman probes was determined empirically by measuring the intensity of the Raman peak (856 cm^{-1}) of a thin film of dried 4-acetaminophen powder on a quartz substrate as it was axially translated. The depth of field determined by the full-width at half-maximum (FWHM) value was 520 and 280 μm, for the high-volume and confocal Raman probes, respectively. The depth of field estimated for the high-volume Raman probe is comparable to the sampling depths of typical Raman probes that report a collection depth in the range of 500 μm [22–24]. Evidently, these values refer to the depth of field in this (reflective) substrate whereas the presence of multiple or diffuse scattering, inherent in biological samples, is prone to increasing the aforementioned dimensions.

The Raman data of the normal and diseased bladder tissue was collected by the confocal and high-volume Raman probes. Raman spectra were acquired in the wavenumber range of 400 to 1,700 cm^{-1} for the fingerprint region from bladder tissue. The acquisition time of each Raman spectrum is 5 s/frame with five frames per tissue site. The laser power used at the tissue surface was ca. 30 mW. The spectral resolution of our Raman system was measured to be 15 cm^{-1} using the FWHM of the aforementioned Raman peak of 4-acetaminophen powder.

Acquisition of Raman spectra from bladder tissue

The present study was conducted at the Ninewells Hospital Medical Research Institute with the approval of the local ethics committee (Ref. No. 10/S1401/29) and was further

monitored by the Research and Development Department of the Tayside Academic Health Science Centre. All patients signed an informed consent permitting the collection of Raman spectra on the tissues resected during transurethral resection of urinary bladder cancer. The ex vivo study described here provides a relatively well-controlled setting (in relation to in vivo investigations) for the direct comparison of the effectiveness of the confocal and high-volume Raman probes. In this study, Raman spectra were acquired from 28 freshly excised tissue samples from a total of 14 patients. In particular, the two Raman spectra were acquired from a site in the grossly normal region and another from the grossly suspicious region of the biopsied tissue, respectively. A photograph of a representative non-muscle invasive high-grade tumor in a bladder diverticulum is given in Fig. 1. The Raman probe was placed in gentle contact with the tissue samples and multiple Raman spectra (5) were obtained from each tissue site within 5 min of tissue resection. As a result, 140 ex vivo Raman spectra (for each probe) were collected from 14 suspected cancer tissue sites and 14 grossly normal sites. Immediately after the Raman acquisitions, the biopsy samples were sent to the histopathology department in 10 % formalin solution for examination by a senior uropathologist. The normal tissue sites as well as the suspected cancer sites (transitional cell carcinoma in situ and squamous cell carcinoma in situ) were confirmed by histopathology in all 14 patients. In order to objectively assess the diagnostic sensitivity and specificity of Raman spectroscopy for cancer tissue classification, the histopathological results were used as the gold standard. The relevant clinical information (class label and spectral dataset) with donor information removed was submitted to the
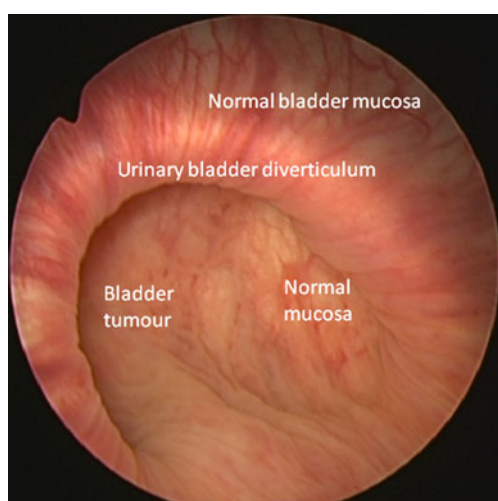
MIT Spectroscopy Laboratory for chemometric analysis and interpretation of the spectroscopic results.

Data analysis

The raw Raman spectra acquired from ex vivo tissue were composed of the intrinsic Raman signals of the various biomarkers, intense autofluorescence backgrounds and various noise components (primarily consisting of shot noise and detector noise). The signals obtained were vertically binned and subsequently subjected to cosmic ray removal [25]. Each Raman spectrum was then selected in the range of 800 to 1,700 cm^{-1} to avoid spurious artifacts arising from the fiber background in the lower wavenumber region.

In this study, to investigate the classification ability of the proposed method between cancer and normal biopsied samples from different patients, we first implemented principal component analysis (PCA) (part of the Statistics Toolbox in MATLAB R2010b (MathWorks, Natick, MA)) on the entire 140 spectra dataset. PCA is a powerful mathematical tool for exploratory data analysis, which employs an orthogonal transformation to convert a set of observations of possibly correlated variables into a set of values of linearly uncorrelated variables called principal components (PC). Importantly, the transformation is performed to account for the maximum variability in the dataset using only a few PC, where each succeeding PC is orthogonal to the previous ones and explains as much as possible of the remaining variance. Here, we have used the PCs for visualization of the important features in the normal and cancerous tissue samples as well as used the corresponding scores in a logistic regression algorithm to quantify the classification accuracy of the proposed approach [26]. A likelihood ratio test was used to determine the PCs most significant for diagnosis. Also, a standard leave-one-out cross-validation protocol [27] was used for the logistic regression analysis. In this protocol, the data from a particular tissue site is eliminated, and logistic regression is used to form a decision line that classifies the remaining tissue sites maximizing agreement with the histopathology diagnoses. The decision line is subsequently used to classify the excluded site. This process is successively applied to each of the [28] sites. The entire analysis procedure is performed separately for the high-volume and confocal Raman datasets.

Results and discussion

Distinguishable Raman bands were observed in both normal and urinary bladder cancer tissue consistent with the features observed by Draga and co-workers [21] albeit with lower signal-to-noise ratio (SNR). The inferior SNR in our confocal Raman spectra (in comparison to our high-volume

Fig. 1 Photograph showing non-muscle invasive high-grade tumor in a bladder diverticulum. The normal epithelium of bladder around and within diverticulum is indicated in the figure. These subtle mucosal changes can be often be missed by white light cystoscopy

Raman spectra as well as that noted in the literature [21]) hinders the ready visualization of the important features, even though the necessary information of the biomarkers is embedded in this dataset. To elucidate this information, PCA was implemented on the dataset consisting of 140 confocal Raman spectra. Figure 2 shows the two most relevant principal components from a diagnostic standpoint, as determined by the likelihood ratio test. These PCs are the first (91.6 %) and third (3.73 %) in terms of explaining the net variance in the dataset—and along with PC 2 (which is largely characteristic of the signal background) accounts for 99.83 % of the total variance. Specifically, PC1 and PC3 highlight the importance of the spectral features at ca. 878, 1,004, 1,184, 1,308, 1,440 (shoulder), and 1,553 cm^{-1}. While a perfect one-to-one correspondence between features observed in principal components and the relevant Raman
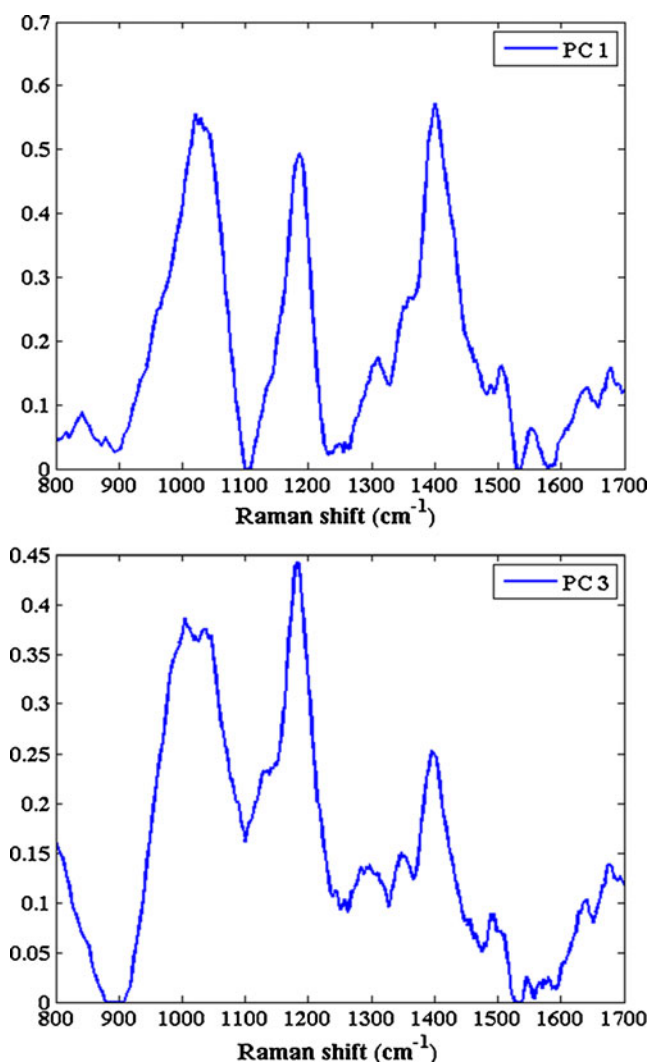
peaks of constituents is difficult to establish, these features can be tentatively assigned to hydroxyproline (878 cm^{-1}), phenylalanine (1,004 cm^{-1}), DNA (cytosine, guanine and adenine) (1,184 cm^{-1}), symmetric CH deformation (1,308 cm^{-1}), CH$_2$ deformation (1,440 cm^{-1}), and tryptophan (1,553 cm^{-1}). It bears mentioning that there may be alternative interpretations and/or contributions from unidentified constituents to these features, as some of the features exhibit different FWHM than typically obtained in standard samples (such as the 1,004 cm^{-1} peak of phenylalanine). Here, we also note that PC1 and PC3 share some common features. Furthermore, we also observe a prominent peak at ca. 1,390–1,405 cm^{-1} (in PC1 as well as in PC3), which was not listed amongst the prominent bands earlier [21]. The origin of this band is unclear at this present time and needs further investigation.

The linear projections' plot of the corresponding scores for PCs 1 and 3 is shown in Fig. 3. As noted above, scores for PC2 were not included in this plot because of its inability to add substantive discriminative ability to the model (this finding is not wholly unexpected, as other investigators have reported that the parameters which contribute most to the fit of spectroscopic data to a model may not be the parameters with the most diagnostic utility [28]). It is evident that very good separation is obtained between a large majority of the normal and cancerous sites. Here, an optimal separation line was constructed by logistic regression analysis (in auto-prediction mode) to distinguish the two data segments, as shown by the black line in Fig. 3. The equation of the line was determined to be:

$$0.0015\,score_1 - 0.0214\,score_3 + 0.9641 = 0 \qquad (1)$$

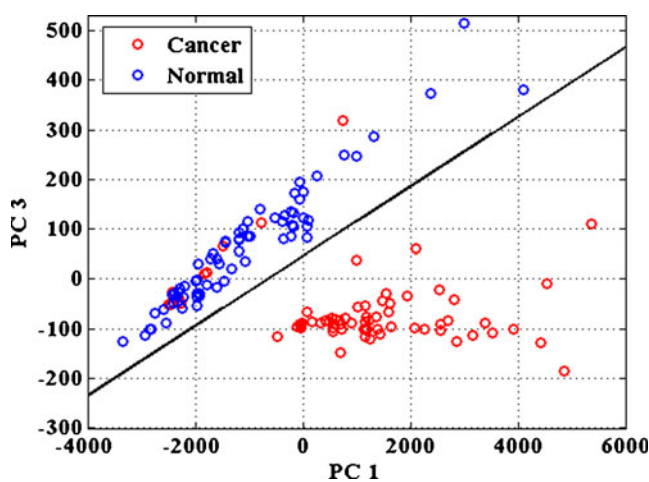In order to more objectively quantify the discrimination ability, leave-one-out cross-validation based logistic

Fig. 2 Plot of principal component (PC) 1 and 3, which provide the most significant discrimination between the tissue types, namely cancerous and normal TURBT samples. These two principal components, along with PC2, explain 99.83 % of the net variance in the dataset

Fig. 3 Logistic regression-based Raman algorithm distinguishing cancerous lesions (red circles) from normal sites (blue circles), as classified by histopathological examination. The x- and y-axes represent the scores corresponding to PC 1 and 3, respectively

regression was subsequently undertaken on the PC scores of the confocal Raman dataset. The results obtained from this analysis are enumerated in the confusion matrix of Table 1. The confusion matrix indicates that we have ten false-negative data points (arising from two sites) and, remarkably, no false-positive points. This translates to sensitivity (Se) of 85.7 %, specificity (Sp) of 100 %, positive predictive value of 100 % and negative predictive value of 87.5 % for the diagnostic algorithm (Table 2). In addition, the overall accuracy is computed to be 92.9 % and the area under the curve (AUC) for the corresponding receiver operating characteristic (ROC) curve (Fig. 4) is 0.91 (where a perfect algorithm has an AUC of 1.00). As leave-one-out cross-validation is widely accepted as a more robust indicator of the true quality of the model in relation to auto-prediction (which often results in over-fitting of the data due to incorporation of noise components), the above results provide a high degree of confidence on the diagnostic value of the proposed method and its potential for classification of prospective ("unknown") samples.

Here, we attribute the inaccuracies in classification (i.e., the ten false negatives from two cancerous sites) to spectroscopy-histopathology registration errors [29, 30]. In other words, the spectroscopic measurements were potentially performed on a grossly normal site of the biopsied tissue whereas the histopathological results were obtained for a marginally different position on the tissue where cancerous cells could be observed. Also, in general, the examination region of the two methodologies (namely, spectroscopy and histopathology) is similar but not identical—and, arguably, spectroscopy is less prone to sampling errors inherent in conventional histopathology assessment.

To further elucidate the effectiveness of incorporating confocality in the Raman probe, we repeated the same data analysis steps (in conjunction with the given histopathology labels) for the high-volume Raman spectral dataset. For the high-volume Raman spectral dataset, the logistic regression algorithm correctly discriminated 60 out of 70 cancerous data points, with the inaccuracies arising from the same two sites as obtained with the confocal Raman probe. However, ten false-positive points are detected by this algorithm in

Table 1 Confusion matrix for leave-one-out cross-validation of logistic regression-based Raman decision algorithm

		Histopathology diagnosis ("Gold Standard")		
Raman spectroscopic diagnosis		Cancer	Normal	Total
	Cancer	60	0	60
	Normal	10	70	80
	Total	70	70	140

Here, the histopathology ("gold standard") diagnosis is provided along the columns whereas the Raman classification is given along the rows

Table 2 Comparison of diagnostic performance of leave-one-out cross-validation Raman algorithm for two sets of assigned labels: the first row provides the performance metrics for true labels whereas the second row gives the same for a representative set of randomly assigned labels

	Sensitivity (%)	Specificity (%)	PPV (%)	NPV (%)	OA (%)
True labels	85.7	100	100	87.5	92.9
Randomized labels	61.1	27.9	47.3	40.4	45

The performance metrics represented here are: sensitivity (%), specificity (%), positive predictive value (PPV) (%), negative predictive value (NPV) (%) and overall accuracy (OA) (%)

contrast to zero such identifications for the confocal Raman dataset. The resultant sensitivity and specificity values are both calculated to be 85.7 % for diagnosis of bladder cancer.

For TURBT procedures, the most important diagnostic parameter is sensitivity, because one would like to identify every single lesion in patient with the disease for treatment or further clinical evaluation. Our sensitivity values (ca. 86 %) for both confocal and high-volume Raman probes are identical and are marginally higher than the sensitivity of the previous high-volume Raman probe-based study [21]. However, the clear contrast in algorithm performance appears in the markedly higher specificity values obtained using our confocal Raman data (100 %). It is worth noting
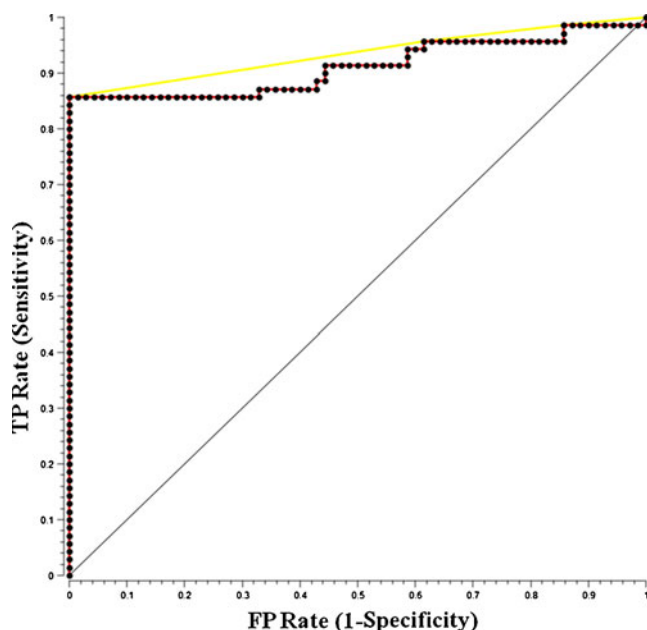
Fig. 4 Receiver operating characteristic (ROC) curve illustrating the ability of confocal Raman spectroscopy to separate cancerous lesions from normal bladder tissue removed by TURBT. The ROC curve of two indistinguishable populations, represented by the *solid black line*, is included for comparison. For this case, the area under the curve (AUC) was calculated to be 0.91 (in comparison, the AUC of the *solid black line* is 0.5)

that the discrepancy in performance metrics between our study and prior investigations may arise from the variations in properties of the specific samples, quality of the histopathology, and/or mathematical analysis. Hence, the more meaningful comparison is between our confocal and high-volume Raman results. The substantive improvement in specificity signifies immense benefits for female patients and patients with a TURBT and/or intravesical adjuvant treatment within 3 months of cystoscopic examination as the false detection rates of PDD are very high (ca. 40 %). Clearly, even if false positives do not pose a life-threatening risk to the patient, the retrieval of additional tissue cores that were not needed is extremely undesirable and serves only to drive up the costs (due to additional time spent in TURBT and the corresponding histopathological examination of unnecessary tissue cores).

The improvement in the specificity of the diagnostic algorithm can be attributed to the incorporation of confocality in our probe design. Based on our empirical depth-of-field value of ca. 280 μm, one can reasonably infer that we are able to more selectively sample the molecular constituents at the surface tissue layers in relation to the high-volume Raman probe used here as well as those used previously [20, 21]. As stated earlier, this depth-of-field value is not necessarily an accurate representation of the corresponding value in a turbid medium (such as biological tissue) where elastic scattering may considerably reduce the penetration and collection depth. In particular, we believe that the confocal probe will help us better diagnose lesion types where only a few layers of cells (a premalignant cancer lesion with mucosal thickness of ca. 100 μm) and carcinoma in situ (which may be composed of only one cell layer, i.e., 15 μm in thickness). As one can readily observe, further reduction in confocal range is probably desirable but would come at the cost of reduction of the intrinsically weak Raman signal. Stone and co-workers have recently established the foundation of such development by designing a gradient index lens-based probe with 147 μm depth of field [31]. Our ex vivo results also compare favorably with their previous fiber-optic probe-based investigations where the authors reported an overall diagnostic accuracy of 84 % in discriminating benign and malignant bladder lesion by acquiring spectra from (snap-frozen) in vitro bladder tissue sample [20]. Our overall accuracy (93 %) is higher in comparison to this value, although presumably discrimination between the benign and malignant lesions is more complex in relation to discrimination between normal and cancer tissue as performed here.

To verify the robustness of the confocal Raman data to potential spurious correlations, we implemented an additional control study. Specifically, the "normal" and "cancer" labels were assigned in a randomized order without accounting for their true labels. Using the scores in a leave-one-out cross-validation logistic regression analysis, we observed that the new overall accuracy values never reached 60 %, even after multiple iterations. A representative set of metrics for one of the iterations is given in Table 2 for comparison with the actual algorithm. This re-iterates the stability of our proposed approach and its robustness to mis-assigned labels and chance correlations in the spectral dataset. Further, due to the high degree of separation obtained using scores for PC 1 and 3, no diagnostic discordance between spectra acquired from the same site was observed. Put differently, despite potential uncertainty in spectroscopic measurements (e.g., shot noise), the lack of fence-sitters in the current dataset ensured that the predicted labels from the replicate spectra (i.e., spectra measured from the same site) were in agreement. This implies that the precision of Raman measurements in the bladder tissue obtained using our confocal Raman probe is sufficient to perform reproducible diagnoses of cancerous lesions.

Conclusion

In this article, we have demonstrated that the specific biochemical information obtained from tissue Raman spectra shows ample promise for the diagnosis of bladder cancer. In particular, we have reported the use of a confocal Raman probe that enables significant enhancement of diagnostic specificity by suppressing spectral information from deeper tissue layers beyond the region of interest. We envision that this finding will be of substantive interest especially given its implications for endoscopic usage, which is the preferred route for the diagnosis and treatment of most urological conditions including urinary bladder cancer.

Furthermore, while the studies performed here provide the foundation for detection of bladder cancer in TURBT samples ex vivo, future research work will be necessary to assess the ability of the technique to provide real-time guidance for TURBT endoscopic procedures in vivo. The sensitivity and specificity of the proposed approach may reduce (slightly) when the Raman algorithm is tested in large-scale studies in more diverse patient populations. Additionally, such studies in the later stages of development will also require the identification and systematic characterization of less common types of lesions not observed in the initial investigations here. Depending on the number of classes required and the complexity of the tissue biochemical composition, we will also assess the performance of other classification algorithms, such as soft independent modeling class analogy [32] and support vector machines [33]. Our long-term goal is to evaluate and translate Raman spectroscopy not only for the real-time detection of cancerous lesions but to be able to discriminate between the grades and stages of such tumors. We expect that the final outcome

of the method application to the clinical setups will be a diagnostic tool that is based on multiple optical/spectroscopic modalities, notably confocal Raman and PDD, where the hybrid combination may establish a new benchmark in terms of both sensitivity and specificity.

Our ongoing scientific research will also focus on several critical aspects that may potentially boost the discrimination ability with minimal change in hardware. One of the focal points is the possibility of combining fingerprint Raman spectra with high-wavenumber information as the latter region has less (adverse) influence of the tissue autofluorescence background. Also, the absence of Raman fiber signals makes the high-wavenumber approach fairly attractive for endoscopic applications [34], despite its lower molecular specificity in comparison to the fingerprint region. Further, selection of the most informative wavelengths (instead of performing full spectral analysis) [35] as well as application of pre-processing steps (such as standard normal variate transformation) that can account for non-analyte-specific baseline variances is currently under investigation. Their proper application is likely to generate a more effective and robust tissue classification algorithm.

References

1. Grasso M (2008) Bladder cancer: a major public health issue. Eur Urol Suppl 7:510–515
2. Kirkali Z, Chan T, Manoharan M, Algaba F, Busch C, Cheng L, Kiemeney L, Kriegmair M, Montironi R, Murphy WM, Sesterhenn IA, Tachibana M, Weider J (2005) Bladder cancer: epidemiology, staging and grading, and diagnosis. Urology 66:4
3. Cheng L, Neumann RM, Bostwick DG (1999) Papillary urothelial neoplasms of low malignant potential. Clinical and biologic implications. Cancer 86:2102
4. Denzinger S, Burger M, Walter B, Knuechel R, Roessler W, Wieland WF, Filbeck T (2007) Clinically relevant reduction in risk of recurrence of superficial bladder cancer using 5-aminolevulinic acid-induced fluorescence diagnosis: 8-year results of prospective randomized study. Urology 69:675
5. Daniltchenko DI, Riedl CR, Sachs MD, Koenig F, Daha KL, Pflueger H, Loening SA, Schnorr D (2005) Long-term benefit of 5-aminolevulinic acid fluorescence assisted transurethral resection of superficial bladder cancer: 5-year results of a prospective randomized study. J Urol 174:2129
6. Mowatt G, N'Dow J, Vale L, Nabi G, Boachie C, Cook JA, Fraser C, Griffiths TR (2011) Aberdeen Technology Assessment Review (TAR) Group. Int J Technol Assess Health Care 27:3–10
7. Hungerhuber E, Stepp H, Kriegmair M, Stief C, Hofstetter A, Hartmann A, Knuechel R, Karl A, Tritschler S, Zaak D (2007) Seven years' experience with 5-aminolevulinic acid in detection of transitional cell carcinoma of the bladder. Urology 69:260
8. Grossman HB, Gomella L, Fradet Y, Morales A, Presti J, Ritenour C et al (2007) J Urol 178:62
9. Botteman MF, Pashos CL, Redaelli A, Laskin B, Hauser R (2003) The health economics of bladder cancer: a comprehensive review of the published literature. PharmacoEconomics 21:1315
10. Mourant JR, Bigio IJ, Boyer J, Conn RL, Johnson T, Shimada T (1995) Spectroscopic diagnosis of bladder cancer with elastic light scattering. Lasers Surg Med 17:350
11. Wang ZG, Durand DB, Schoenberg M, Pan YT (2005) Fluorescence guided optical coherence tomography for the diagnosis of early bladder cancer in a rat model. J Urol 174:2376
12. Brereton RG (2007) Applied chemometrics for scientists
13. Nogueira GV, Silveira L, Martin AA, Zangaro RA, Pacheco MT, Chavantes MC, Pasqualucci CA (2005) Raman spectroscopy study of atherosclerosis in human carotid artery. J Biomed Opt 10:031117
14. Haka AS, Shafer-Peltier KE, Fitzmaurice M, Crowe J, Dasari RR, Feld MS (2005) Diagnosing breast cancer by using Raman spectroscopy. Proc Natl Acad Sci U S A 102:12371
15. Ramasamy M, Shafer K, Perelman L, Wu J, Chen K, Deinum G, Fitzmaurice M, Myles J, Crowe J, Dasari RR, Feld MS (1998) Photochem Photobiol 67:15–22
16. Saha A, Barman I, Dingari NC, McGee S, Volynskaya Z, Galindo LH, Liu W, Plecha D, Klein N, Dasari RR, Fitzmaurice M (2011) Raman spectroscopy: a real-time tool for identifying microcalcifications during stereotactic breast core needle biopsies. Biomed Opt Express 2:2792
17. Bodanese B, Silveira L Jr, Albertini R, Zangaro RA, Pacheco MT (2010) Differentiating normal and basal cell carcinoma human skin tissues in vitro using dispersive Raman spectroscopy: a comparison between principal components analysis and simplified biochemical models. Photomed Laser Surg 28(Suppl 1):S119
18. Draga RO, Grimbergen MC, Kok ET, Jonges TN, Bosch JL (2009) Predictors of false positives in 5-aminolevulinic acid-induced photodynamic diagnosis of bladder carcinoma: identification of patient groups that may benefit most from highly specific optical diagnostics. Urology 74:851
19. Crow P, Uff JS, Farmer JA, Wright MP, Stone N (2004) The use of Raman spectroscopy to identify and characterize transitional cell carcinoma in vitro. BJU Int 93:1232
20. Crow P, Molckovsky A, Stone N, Uff J, Wilson B, WongKeeSong LM (2005) Assessment of fiberoptic near-infrared Raman spectroscopy for diagnosis of bladder and prostate cancer. Urology 65:1126
21. Draga RO, Grimbergen MC, Vijverberg PL, van Swol CF, Jonges TG, Kummer JA, Ruud Bosch JL (2010) In vivo bladder cancer diagnosis by high-volume Raman spectroscopy. Anal Chem 82:5993
22. Motz JT, Hunter M, Galindo LH, Gardecki JA, Kramer JR, Dasari RR, Feld MS (2004) Optical fiber probe for biomedical Raman spectroscopy. Appl Opt 43:542
23. Motz JT, Gandhi SJ, Scepanovic OR, Haka AS, Kramer JR, Dasari RR, Feld MS (2005) Realtime Raman system for in vivo disease diagnosis. J Biomed Opt 10:031113
24. Puppels GJ, Bakker Schut TC, Caspers PJ, Wolthuis R, van Aken M, van der Laarse A (2001) In vivo Raman spectroscopy. In: Handbook of Raman spectroscopy: from research laboratory to the process line. Marcel Dekker, New York 549–574
25. Barman I, Kong CR, Singh GP, Dasari RR (2011) Effect of photobleaching on calibration model development in biological Raman spectroscopy. J Biomed Opt 16:011004
26. Dingari NC, Horowitz GL, Kang JW, Dasari RR, Barman I (2012) Raman spectroscopy provides a powerful diagnostic tool for accurate determination of albumin glycation. PLoS One 7:e32406
27. Barman I, Dingari NC, Rajaram N, Tunnell JW, Dasari RR, Feld MS (2011) Rapid and accurate determination of tissue optical properties using least-squares support vector machines. Biomed Opt Exp 2(3):592–599

28. Fitzmaurice M (2000) Principles and pitfalls of diagnostic test development: implications for spectroscopic tissue diagnosis. J Biomed Opt 5:119

29. Motz JT, Fitzmaurice M, Miller A, Gandhi SJ, Haka AS, Galindo LH, Dasari RR, Kramer JR, Feld MS (2006) In vivo Raman spectral pathology of human atherosclerosis and vulnerable plaque. J Biomed Opt 11(2):021003

30. Dingari NC, Barman I, Saha A, McGee S, Galindo LH, Liu W, Plecha D, Klein N, Dasari RR, Fitzmaurice M (2012) Development and comparative assessment of Raman spectroscopic classification algorithms for lesion discrimination in stereotactic breast biopsies with microcalcifications. J Biophotonics. doi:10.1002/jbio.201200098

31. Day JC, Bennett R, Smith B, Kendall C, Hutchings J, Meaden GM, Born C, Yu S, Stone N (2009) A miniature confocal Raman probe for endoscopic use. Phys Med Biol 54:7077

32. Myakalwar AK, Sreedhar S, Barman I, Dingari NC, Venugopal Rao S, Prem Kiran P, Tewari SP, Manoj Kumar G (2011) Laser-induced breakdown spectroscopy-based investigation and classification of pharmaceutical tablets using multivariate chemometric analysis. Talanta 87:53–59

33. Dingari NC, Barman I, Myakalwar AK, Tewari SP, Gundawar MK (2012) Incorporation of support vector machines in the LIBS toolbox for sensitive and robust classification amidst unexpected sample and system variability. Anal Chem 84:2686–2694

34. Lin K, Cheng DL, Huang Z (2012) Optical diagnosis of laryngeal cancer using high wavenumber Raman spectroscopy. Biosens Bioelectron 35:213–217

35. Dingari NC, Barman I, Kang JW, Kong CR, Dasari RR, Feld MS (2011) Wavelength selection based nonlinear calibration for transcutaneous blood glucose sensing using Raman spectroscopy. J Biomed Opt 16:087009